

The approximation method for calculation of the exponent of the gluon distribution- λ_g and the structure function- λ_S at low x

G.R.Boroun* and B.Rezaie

Physics Department, Razi University, Kermanshah 67149, Iran

(Dated: December 3, 2024)

We present a set of formulae using the solution of the QCD Dokshitzer-Gribov-Lipatov-Altarelli-parisi (DGLAP) evolution equation to the extract of the exponent λ_g gluon distribution and λ_S structure function from the Regge- like behavior at low x . The exponents are found to be independent of x and to increase linearly with $\ln Q^2$ and compared with the most data from H1 Collaboration. We also calculated the structure function $F_2(x, Q^2)$ and the gluon distribution $G(x, Q^2)$ at low x assuming the Regge- like behavior of the gluon distribution function at this limit and compared with NLO QCD fit to the H1 data, two Pomeron fit, multipole Pomeron exchange fit and MRST (A.D.Martin, R.G.Roberts, W.J.Stirling and R.S.Thorne), DL(A.Donnachie and P.V.Landshoff), NLO-GRV(M.Gluk, E.Reya and A.Vogt) fit results, respectively.

1 Introduction

The Knowledge of the deep inelastic scattering (DIS) structure functions at small values of the Bjorken scaling variable x is interesting for understanding the inner structure of hadrons. Of great relevance is the determination of the gluon density at low- x , where gluons are expected to be dominant, because it could be a test of perturbative quantum chromodynamic (PQCD) or a probe of new effects, and also because it is the basic ingredient in many other calculations of different high energy hadronic processes.

The behavior of the proton structure function $F_2(x, Q^2)$ at small x reflects the behavior of the gluon distribution, since the gluon is by far the dominant parton in this regime. At small x , only the structure function F_2 is measured. On the other hand, the gluon distribution cannot be measured directly from experiments. It is, therefore, important to measure the gluon distribution $G(x, Q^2)$ indirectly from the proton structure function $F_2(x, Q^2)$ through the transition $g \rightarrow q\bar{q}$. Here the representation for the gluon distribution $G(x) = xg(x)$ is used, where $g(x)$ is the gluon density.

In PQCD, the high- Q^2 behavior of DIS is given by the Dokshitzer- Gribov- Lipatov- Altarelli- Parisi (DGLAP) evolution equations [1]. In the double asymptotic limit (large energies, i.e. small- x and large photon virtualities Q^2), the DGLAP evolution equations can be solved [2] and structure function is expected to rise approximately like a power of x towards small- x . This steep rise of $F_2(x, Q^2)$ towards low- x observed at HERA [3], also indicates in PQCD a similar rise of the gluon towards low- x . This similar behavior

*boroun@razi.ac.ir

predicts a steep power law behavior for gluon distribution. Accordingly the approximate solutions of DGLAP evolution equations are reported in recent years [4,5] with considerable phenomenological success.

The small- x region of DIS offerees a unique possibility to explore the Regge limit of PQCD [6,7]. This theory is successfully described by the exchange of a particle with appropriate quantum numbers and the exchange particle is called a Regge pole. Phenomenologically, the Regge pole approach to deep inelastic scattering implies that the structure functions are sums of powers in x , modulus logarithmic terms, each with a Q^2 - dependent residue factor. This model gives the following parametrization of the deep inelastic scattering structure function $F_2(x, Q^2)$ at small x , $F_2(x, Q^2) = \sum_i A_i(Q^2)x^{-\lambda_i}$, that the singlet part of the structure function is controlled by pomeron exchange at small x . The rapid rise in Q^2 of the structure functions was considered as a sign of departure from the standard Regge behavior. The reason was that the HERA data, when fitted by a single "Regge- pomeron" term $\sim x^{-\lambda_S}$, where λ_S is the pomeron intercept minus one, show that $\lambda_S = \frac{d \ln F_2(x, Q^2)}{d \ln \frac{1}{x}}$ definitely rises with Q^2 .

The Regge behavior of the structure function in the large- Q^2 region reflects itself in the small- x behavior of the quark and the antiquark distributions. Thus the Regge behavior of the sea quark and antiquark distribution for small- x is given by $q_{sea}(x) \sim x^{-\alpha_p}$ corresponding to a pomeron exchange with an intercept of $\alpha_p = 1$. But the valance quark distribution for small- x given by $q_{val}(x) \sim x^{-\alpha_R}$ corresponds to a Reggeon exchange with an intercept of $\alpha_R = 1/2$. The small x behavior of the structure functions is driven by gluon through the $g \rightarrow q\bar{q}$ transition and the increase of gluon distributions with decreasing x implies a similar increase of the deep inelastic lepton- proton scattering structure function F_2 as the Bjorken parameter x decreases, so we expect $g(x) \sim 1/x$. The x - dependence of the parton densities given above is often assumed at moderate- Q^2 .

In principle, the HERA data should determine the small x behavior of gluon and sea quark distribution. Roughly speaking the data on the singlet part of the structure function F_2 constrain the sea quarks and the data on the slope $dF_2/d \ln Q^2$ determine the gluon density. For example if we take:

$$F_2 \sim xS \sim A_S x^{-\lambda_S}, \quad (1)$$

and

$$\frac{dF_2}{d \ln Q^2} \sim xg \sim A_g x^{-\lambda_g}, \quad (2)$$

then we might expect to determine λ_S and λ_g . In the DGLAP formalism the gluon splitting functions are singular as $x \rightarrow 0$. Thus the gluon distribution will become large as $x \rightarrow 0$, and its contribution to the evolution of the parton distribution becomes dominant. In particular the gluon will drive the quark singlet distribution, and hence the structure function F_2 becomes large as well, the rise increasing in steepness as Q^2 increases.

The rapid rise in Q^2 of the gluon distribution at small x , observed at HERA, shows by[8]:

$$xg(x, Q^2) = A_g x^{-\lambda_g}, \quad (3)$$

where λ_g is the pomeron intercept minus one. In the double asymptotic limit (large energies. i.e. small x , and large photon virtualities Q^2) the DGALP evolution equations [1] can be solved [2] and F_2 is expected to rise approximately like a power of x towards low x . In leading order the DGLAP gluon distribution solution gives [2]:

$$\lambda_g = \left[\frac{12 \ln(\frac{t}{t_0})}{\beta_0 \ln(\frac{1}{x})} \right]^{1/2}, \quad (4)$$

where $t = \ln(\frac{Q^2}{\Lambda^2})$, $t_0 = \ln(\frac{Q_0^2}{\Lambda^2})$ (that Λ is the QCD cut-off parameter) and $\beta_0 = \frac{33-2N_f}{3}$, N_f being the number of flavours. This steep behavior of the gluon generates a similar steep behavior of F_2 at small x , Eq.(1), where $\lambda_S = \lambda_g - \epsilon$ (i.e. $\lambda_S \neq \lambda_g$ in next- to- leading order analysis). At small x terms in $\ln(1/x)$ are becoming large and the conventional leading $\ln Q^2$ summation of the DGLAP equations does not account for this. It may also be necessary to sum leading $\ln(1/x)$ terms. Such a summation is performed by the BFKL [9] equation. To leading order in $\ln(1/x)$ with fixed α_s , this predicts a steep power law behavior $xg(x, Q^2) \sim x^{-\lambda_g}$ where $\lambda_g = \frac{3\alpha_s}{\pi} 4 \ln 2 \simeq 0.5$ (for $\alpha_s \simeq 0.2$, as appropriate for $Q^2 \sim 4 \text{ GeV}^2$).

For $Q^2 \leq 1 \text{ GeV}^2$, the simplest Regge phenomenology predicts that the value of $\lambda_S = \alpha_{\mathbb{P}}(0) - 1 \simeq 0.08$ is consistent with that of hadronic Regge theory [3,10] where $\alpha_{\mathbb{P}}(0)$ is described soft pomeron dominant with its intercept slightly above unity (~ 1.08), whereas for $Q^2 \geq 1 \text{ GeV}^2$ the slope rises steadily to reach a value greater than 0.3 by $Q^2 \approx 100 \text{ GeV}^2$ where hard pomeron is dominant. This larger value of λ_S is not so far from that expected using BFKL [9] ideas. Indeed, the BFKL equation can be viewed as a method for the calculation of the hard or perturbative Pomeron trajectory (in contrast to the soft or non- perturbative Pomeron of hadronic physics with intercept around 1.08 [11]). There is some other authors [10] which extended their Regge model adding a hard Pomeron with intercept 1.44, which allows them to describe the low x HERA data up to Q^2 values of a few hundred GeV^2 .

Our goal in this work is to present an approximate analytical solution for the singlet structure function and the gluon distribution as we should be able to calculate λ_S and λ_g in the next- to- leading order DGLAP equation, valid to be at low- x . In order to do this, the DGLAP evolution equations are calculated neglecting the quark distribution. The approach, using the Regge and the Regge- like behavior for singlet and gluon distribution respectively, has been applied in this paper. We test its validity comparing it with that of H1 Collaboration and attempt to see how the predictions for singlet exponent are compared with the experimental data [3].

The formulation of the problem in NLO-DGLAP evolution equations for calculation λ_g and λ_S are given in Sections.2 and 3. Finally in Secion.4, the numerical results are given, leading to discussion and conclusions.

2. Calculation of λ_g based on Regge- like behavior gluon distribution function

Neglecting the quark singlet part, the DGLAP equation for the gluon evolution in the NLO can be written as [12]:

$$Q^2 \frac{\partial G}{\partial Q^2} = \frac{\alpha_s}{2\pi} \int_x^1 [P_{gg}^1(z) + \frac{\alpha_s}{2\pi} P_{gg}^2(z)] G(\frac{x}{z}, Q^2) dz, \quad (5)$$

where $P_{gg}^1(z)$ and $P_{gg}^2(z)$ are the LO and NLO Altarelli- Parisi splitting kernels [1,12]. The running coupling constant $\alpha_s(Q^2)$ has the approximate analytical form in NLO:

$$\frac{\alpha_s(Q^2)}{2\pi} = \frac{2}{\beta_0 \ln(\frac{Q^2}{\Lambda^2})} [1 - \frac{\beta_1 \ln \ln(\frac{Q^2}{\Lambda^2})}{\beta_0^2 \ln(\frac{Q^2}{\Lambda^2})}], \quad (6)$$

where $\beta_0 = \frac{1}{3}(33 - 2N_f)$ and $\beta_1 = 102 - \frac{38}{3}N_f$ are the one- loop (LO) and the two- loop (NLO) correction to the QCD β - function, N_f being the number of active quark flavours ($N_f = 4$). To find an analytic solution, we note that the splitting kernels $P_{gg}^1(x)$ and $P_{gg}^2(x)$ at the small x limit are [13,14]:

$$P_{gg}^1(x) = 2C_A [\frac{x}{(1-x)_+} + \frac{1-x}{x} + x(1-x)] + \delta(1-x) \frac{(11C_A - 4N_f T_R)}{6}, \quad (7)$$

$$P_{gg}^2(x) = \frac{(12C_F N_f T_R - 46C_A N_f T_R)}{9x} + N_f T_R (\frac{-61}{9} C_F + \frac{172}{72} C_A) + C_A^2 (\frac{1643}{54} - \frac{22}{3} \zeta(2) - 8\zeta(3)). \quad (8)$$

Where the casimir operators of colour SU(3) are defined as:

$$C_A = 3, \quad C_F = \frac{4}{3}, \quad T_R = \frac{1}{2}, \quad (9)$$

and $[f(x)]_+ \equiv f(x) - \delta(1-x) \int_0^1 f(y) dy$. Using Eqs.(7-9) in Eq.(5) and carrying out the integration we get:

$$\frac{dG(x, t)}{dt} = \frac{3\alpha_s}{\pi} I_{\lambda_g} G(x, t) + (\frac{\alpha_s}{2\pi})^2 T_{\lambda_g} G(x, t), \quad (10)$$

where

$$T_{\lambda_g} = \frac{(12C_F N_f T_R - 46C_A N_f T_R)}{9\lambda_g} (1 - x^{\lambda_g}) + [N_f T_R (\frac{-61}{9} C_F + \frac{172}{72} C_A) + C_A^2 (\frac{1643}{54} - \frac{22}{3} \zeta(2) - 8\zeta(3))] \frac{1 - x^{1+\lambda_g}}{1 + \lambda_g}, \quad (11)$$

$$I_{\lambda_g} = \left(\frac{11}{12} - \frac{N_f}{18}\right) + \ln(1-x) + \int_x^1 dz \left[\frac{z^{1+\lambda_g} - 1}{1-z} + (1-z)(z^{1+\lambda_g} + z^{\lambda_g-1}) \right]. \quad (12)$$

and

$$\begin{aligned} & \int_x^1 dz \left[\frac{z^{1+\lambda_g} - 1}{1-z} + (1-z)(z^{1+\lambda_g} + z^{\lambda_g-1}) \right] \\ &= \frac{2}{2+\lambda_g}(1-x^{2+\lambda_g}) - (1-x) - \frac{1}{2}(1-x^2) \\ & \quad + \frac{1}{\lambda_g}(1-x^{\lambda_g}) - \frac{1}{1+\lambda_g}(1-x^{1+\lambda_g}) \\ & + \sum_{N=4}^{\infty} \left[\frac{1}{N+\lambda_g}(1-x^{N+\lambda_g}) - \frac{1}{N-1}(1-x^{N-1}) \right]. \end{aligned} \quad (13)$$

Eq.(10) can be rearranged as:

$$\frac{dG(x,t)}{dt} = \left(\frac{3\alpha_s}{\pi} I_{\lambda_g} + \frac{\alpha_s^2}{4\pi^2} T_{\lambda_g} \right) G(x,t). \quad (14)$$

We note that exponent λ_g is given as the derivative

$$\lambda_g = \left. \frac{\partial \ln G(x,t)}{\partial \ln \frac{1}{x}} \right|_{t=\text{constant}}. \quad (15)$$

To obtain an expression for λ_g we first differentiate Eq.(14) with respect to $\ln(1/x)$ and then integrate from t_0 to t . Finally, as $x \rightarrow 0$, we retaining only its leading terms, i.e., the approximate analytical solution is given as follows:

$$\lambda_g G(x,t) - \lambda_{g_0} G(x,t_0) = \int_{t_0}^t G(x,t) \left(\frac{3\alpha}{\pi} - \frac{61\alpha^2}{9\pi^2} \right) dt. \quad (16)$$

where $\lambda_{g_0} (= \frac{\partial \ln G(x,t_0)}{\partial \ln \frac{1}{x}})$ is the exponent at the starting scale t_0 while $G(x,t_0)$ is the input gluon distribution. On the other hand, Eq.(14) in low- x has the explicit form:

$$\ln \frac{G(x,t)}{G(x,t_0)} = \int_{t_0}^t \left(\frac{3\alpha}{\pi} - \frac{61\alpha^2}{9\pi^2} \right) \frac{1-x^{\lambda_g}}{\lambda_g} dt. \quad (17)$$

Hence, we obtain an approximation expression for λ_g as

$$\begin{aligned} & \ln \frac{\lambda_{g_0}}{\lambda_g - x^{\lambda_g} \int_{t_0}^t x^{-\lambda_g} \left(\frac{3\alpha}{\pi} - \frac{61\alpha^2}{9\pi^2} \right) dt} \\ &= \int_{t_0}^t \left(\frac{3\alpha}{\pi} - \frac{61\alpha^2}{9\pi^2} \right) \frac{1-x^{\lambda_g}}{\lambda_g} dt. \end{aligned} \quad (18)$$

The low x behavior of F_2 at fixed Q^2 is studied locally by the measurement of the derivative $\lambda_S \equiv -(\partial \ln F_2 / \partial \ln x)_{Q^2}$ as function of x and Q^2 [3]. The new shifted vertex and the published data agree well in the overlap region. The derivative $\lambda(x, Q^2)$ is independent of x for $x < 0.01$ to within the experimental accuracy. This implies that x dependence of F_2 at low x is consistent with a power law $F_2 \sim x^{-\lambda_S(Q^2)}$, for fixed Q^2 . As, $\lambda_S(Q^2)$ rises approximately linearly with $\ln Q^2$. The rise of the proton structure function towards small x has been discussed since the gluon distribution is dominated within the proton at low x . So, the function λ_g also rises approximately linearly with $\ln Q^2$. This dependence can be represented as $\lambda_g(Q^2) = b_g \ln[Q^2/\Lambda^2]$ where b_g is a constant. Hence, after the determination of λ_g , we can calculate gluon distribution function from Eq.(17) and compare our results with those of other authors. We take all our inputs from NLO- GRV[15] and H1 collaboration [16] and MRST2001[17].

3. Calculation of λ_S based on Regge-like behavior of the structure function

The main task is the determination of singlet exponent structure function from the NLO-DGLAP evolution equations. As it can be seen, for small- x , the gluon term, dominates over the scaling violation of F_2 . Neglecting the quark, the DGLAP evolution equation for the singlet structure function has the form:

$$\frac{dF_2^S}{dt} = \frac{\alpha_s}{2\pi} \int_x^1 dz (2N_f P_{qg}^1(z) + \frac{\alpha_s}{2\pi} P_{qg}^2(z)) G(\frac{x}{z}, Q^2). \quad (19)$$

where $P_{qg}^1(z)$ and $P_{qg}^2(z)$ are the LO and NLO Altarelli- Parisi splitting kernels [1,12]. The splitting kernels $P_{qg}^1(x)$ and $P_{qg}^2(x)$ can be written as [12,13]:

$$P_{qg}^1(x) = \frac{1}{2}[x^2 + (1-x)^2], \quad (20)$$

and

$$\begin{aligned} P_{qg}^2(x) = & C_F N_f T_R \{ 4 - 9x - (1-4x) \ln x - (1-2x) \ln^2 x + 4 \ln(1-x) + [2 \ln^2(\frac{1-x}{x}) \\ & - 4 \ln(\frac{1-x}{x}) - \frac{2}{3} \pi^2 + 10] P_{qg}(x) \} + C_A N_f T_R \{ \frac{182}{9} + \frac{14}{9} x \\ & + \frac{40}{9x} + (\frac{136}{3} x - \frac{38}{3}) \ln x - 4 \ln(1-x) - (2+8x) \ln \ln^2 x + 2 P_{qg}(-x) S_2(x) \\ & + [-\ln^2 x + \frac{44}{3} \ln x - 2 \ln^2(1-x) + 4 \ln(1-x) + \frac{\pi^2}{3} - \frac{218}{9}] P_{qg}(x) \} \end{aligned} \quad (21)$$

where $P_{qg}(x) = x^2 + (1-x)^2$ and $S_2(x) = \int_{\frac{x}{1+x}}^{\frac{1}{1+x}} \frac{dz}{z} \ln(\frac{1-z}{z})$. The small- x limit of the next-to- leading order splitting function for the evolution of the singlet quark is then [14]:

$$P_{qg}^2(x) \longrightarrow \frac{\alpha_s}{2\pi} \frac{40 C_A N_f T_R}{9x}. \quad (22)$$

Based on the Regge- like behavior of the gluon distribution, let us putting Eq.(3) in Eq.(19). Thus, Eq.(19) is reduced to:

$$\begin{aligned} \frac{dF_2^S}{dt} = & \frac{2\alpha_s}{\pi} G(x, t) \left[\frac{2}{3 + \lambda_g} (1 - x^{3+\lambda_g}) + \frac{1}{1 + \lambda_g} (1 - x^{1+\lambda_g}) - \frac{2}{2 + \lambda_g} (1 - x^{2+\lambda_g}) \right] \\ & + \frac{120}{18} \left(\frac{\alpha_s}{\pi} \right)^2 G(x, t) \frac{1 - x^{\lambda_g}}{\lambda_g}. \end{aligned} \quad (23)$$

or

$$\begin{aligned} \frac{dF_2}{dt} = & \frac{5\alpha_s}{9\pi} G(x, t) \left[\frac{2}{3 + \lambda_g} (1 - x^{3+\lambda_g}) + \frac{1}{1 + \lambda_g} (1 - x^{1+\lambda_g}) - \frac{2}{2 + \lambda_g} (1 - x^{2+\lambda_g}) \right] \\ & + \frac{50}{27} \left(\frac{\alpha_s}{\pi} \right)^2 G(x, t) \frac{1 - x^{\lambda_g}}{\lambda_g}. \end{aligned} \quad (24)$$

Therefore, the proton structure function in the low- x region should be determined from Eq.(24). To continue, we want to calculate the exponent λ_S as the derivative

$$\lambda_S = \left. \frac{\partial \ln F_2(x, t)}{\partial \ln \frac{1}{x}} \right|_{t=cte}, \quad (25)$$

and compare the prediction with the $H1$ data [3] where the measurement of the exponent in a large kinematical domain at low x , $3.10^{-5} \leq x \leq 0.2$ and $1.5 \leq Q^2 \leq 150 \text{ GeV}^2$ has been reported. The exponent λ_S being directly measurable from the structure function data can give us helpful insight into the behavior of the structure function at low- x . In order to find solution for λ_S we first differentiate Eq.(24) with respect to $\ln 1/x$ and then integrate from t_0 to t . Finally we obtain:

$$\begin{aligned} \lambda_S F_2(x, t) - \lambda_{S_0} F_2(x, t_0) = & \frac{0.555}{\pi} \int_{t_0}^t \alpha_s G(x, t) \left[\left(\frac{2\lambda_g}{3 + \lambda_g} (1 - x^{3+\lambda_g}) + \frac{\lambda_g}{1 + \lambda_g} (1 - x^{1+\lambda_g}) \right. \right. \\ & \left. \left. - \frac{2\lambda_g}{2 + \lambda_g} (1 - x^{2+\lambda_g}) \right) + (2x^{3+\lambda_g} + x^{1+\lambda_g} - 2x^{2+\lambda_g}) \right] dt \\ & + \frac{1.852}{\pi^2} \int_{t_0}^t \alpha_s^2 G(x, t) dt \end{aligned} \quad (26)$$

which defines the solution for λ_S . In this equation $\lambda_{S_0} = \frac{\partial \ln F_2(x, t_0)}{\partial \ln \frac{1}{x}}$ and $F_2(x, t_0)$ is input structure function at the starting scale t_0 . In calculations, we use the structure function (Eq.24) and take the gluon distribution (Eq.16) for singlet exponent.

4. Discussion and Conclusions

In this research we employed the Regge- like behavior of singlet structure and gluon distribution function to calculate exponent λ_S singlet and λ_g gluon based on NLO- DGLAP evolution equations. Also, the singlet structure function and the gluon distribution are calculated at the x and Q^2 range of HERA data. We compared our results with the experimental results from $H1$ collaboration [3]. The results of calculations are shown in

Figs.1-8. For our calculation the Λ is equal to 292 MeV corresponding to Ref.[3].

In Fig.1 we show λ_g calculated from Eq.(18) as a function of x at four different fixed Q^2 values from 12 to 25 GeV^2 . We observe that the derivative λ_g is almost independent of x and consistent with the HERA data and compared with the MRST2001[17] fit. In Fig.2 we observe the exponent rises almost linearly with $t(= \ln(Q^2/\Lambda^2))$. This behavior is consistent with HERA data.

In order to test the validity of our obtained exponent gluon distribution, we calculate the gluon distribution functions using Eq.(17) and compare them with the theoretical predictions starting with the evolution at $Q_0^2 = 5 \text{ GeV}^2$. As it can be seen in Fig.3, the values of $G(x, Q^2)$ increase as x decreases. Comparing these values with those of NLO-GRV [15], Donnachie & Landshoff (DL)[18] and MRST2001 [17] we can observe that these gluon distribution function values are in agreement with the input parameterization at low x . In all cases the gluon distribution functions are increases as Q^2 is increased.

In Fig.4 we show λ_S calculated from Eq.(26) as a function of x at four different fixed Q^2 values. we observe at low x the derivative λ_S is almost independent of x consistent with the $H1$ [3] data explored in this range. This implies that the x dependence of F_2 at low x is consistent with a power law, $F_2 \propto x^{-\lambda_S}$, for fixed Q^2 . Since quark contributions to the scaling violation of F_2 are negligible, the low x behavior is driven solely by the gluon field. At larger x the transition to the valence- quark region causes a strong dependence of λ_S on x as indicated by the NLO-QCD curves in Fig.1 of Ref.[3].

In Fig.5 we compare our predictions with $H1$ [3] data for λ_S as a function of Q^2 at six different fixed x values. The derivative λ_S of the proton singlet structure function is observed to rise approximately logarithmically with Q^2 . It can be represented by a function $\lambda_S(Q^2)$ which is independent of x within the experimental accuracy. Of course, there is a mild x dependency within the experimental total errors. This is consistent with the slopes extracted by Desgrolard *et al* [19]. At this point it is worth nothing that though the x - slope is often assumed to be constant for small $x \leq 0.01$, there is no theoretical justification for a constant $\lambda_S(Q^2)$ at each fixed Q^2 . In fact there are many models of structure functions that predict a varying $\lambda_S(Q^2)$ with x . For example, in the two Pomeron model, $\lambda_S(Q^2)$ has been shown to vary significantly with x [20]. Similarly in the generalized double asymptotic scaling (DAS) [21], a tiny x dependence is developed in the effective slopes $\lambda_S(Q^2)$ of the structure functions. The Regge- based models [22] also predict a decrease of $\lambda_S(Q^2)$ for fixed Q^2 as $x \rightarrow 0$.

The function $\lambda_S(Q^2)$ is determined from fits of the form $F_2(x, Q^2) = A_S(Q^2)x^{-\lambda_S}$ to our structure function data, restricted to the region $x \leq 0.01$. The results for $A_S(Q^2)$ and $\lambda_S(Q^2)$ are presented in Figs.6 and 7. The coefficients $A_S(Q^2)$ are approximately independent of Q^2 with a mean value of 0.192 (see Fig.7). As can be seen in Fig.6, $\lambda_S(Q^2)$ has an approximate linear rise with $\ln Q^2$. It can be observed from these figures that using Eq.(26) one can reach the good agreement with the $H1$ Collaboration data [3] at low x . In Regge theory the high energy behavior of hadron-hadron and photon-hadron total cross section is determined by the pomeron intercept $\alpha_P = 1 + \lambda$, and is given by $\sigma_{\gamma(h)p}^{tot}(\nu) \sim \nu^\lambda$. This behavior is also valid for a virtual photon for $x \ll 1$, leading to the well known

behavior, $F_2 \sim x^{-\lambda}$, of the structures at fixed Q^2 and $x \rightarrow 0$. The power λ is found to be either $\lambda \sim 0.08$ or $\lambda \sim 0.3$. The first value corresponds to the soft Pomeron and the second value the hard (Lipatov) Pomeron intercept [18].

However, due to the existence of absorptive corrections, this is not the true Pomeron intercept (sometimes referred to as "bare" Pomeron), but rather an effective one. The bare Pomeron intercept is in fact substantially larger than $1 + \lambda_0$. Indeed the relative contribution of the most important absorptive corrections decreases quite rapidly when Q^2 increases (like Q^{-2} for the eikonal ones), so that as $Q^2 \rightarrow \infty$ we see a Pomeron intercept which is close to the bare Pomeron much larger than the soft Pomeron. This consideration have prompted us to use a low x behavior of the structure function of the form:

$$F_2(x, Q^2) \sim x^{-\lambda(Q^2)}; \quad \lambda(Q^2) = \lambda_0 \left(1 + \frac{2Q^2}{Q^2 + d}\right), \quad (27)$$

where λ_0 and d are free parameters [23]. In Fig.6 we observe this behavior.

The Form $x^{-\lambda_g}$ for the gluon parametrization at small x is suggested by Regge behavior, but whereas the conventional Regge exchange is that of the soft Pomeron, with $\lambda_g \sim 0.0$, one may also allow for a hard Pomeron with $\lambda_g \sim 0.5$. The form $x^{-\lambda_S}$ in the sea quark parametrization comes from similar considerations since, at small x , the process $g \rightarrow q\bar{q}$ dominates the evolution of the sea quarks. Hence the fits to early HERA data have as a constraint $\lambda_S = \lambda_g$. However, one only expects this once Q^2 is large enough for the effect of DGLAP evolution to be seen, hence it may not be a reasonable constraint at $Q^2 = Q_0^2$. Furthermore, the exact solution of the DGLAP equations predicts that $\lambda_S = \lambda_g - \epsilon$. The data at low x are now of sufficient precision that λ_S and λ_g to be separate free parameters, as in the MRST fits. One notes that the gluon low x slope has become valence-like; however, this quickly changes as Q^2 increases, such that λ_S and λ_g become equal at low Q^2 and for larger Q^2 , $\lambda_g > \lambda_S$, as expected by PQCD [4,11]. The evolution of the parameters λ_S and λ_g with Q^2 observe in Figs.2 and 6. In these figures we see the differences between the values $\lambda_S \sim 0.30$ and $\lambda_g \sim 0.37$ are consistent to PQCD. This difference shows that at low x the gluon distribution is more singular than the quark distribution. In other words the gluon is by far the most dominant parton and F_2 is essentially given by the singlet sea quark distribution which is driven by the gluon (through the $g \rightarrow q\bar{q}$ splitting process) as $x \rightarrow 0$. The small changes in the quark distribution exponent can be accompanied by large changes in the gluon distribution exponent.

In Fig.8 the calculation of the structure function $F_2(x, Q^2)$ at low x is shown as a function of x . In this figure we observe a continuous rise towards low x . From the figures it can be seen that the results are well described for all Q^2 - values by the NLO QCD fit, as is discussed in detail in section 7.2 of Ref.[16]. The $\ln Q^2$ dependence of F_2 is observed to be non- linear. It can be well described by a quadratic expression

$$F_2(x, Q^2) = a(x) + b(x) \ln Q^2 + c(x) (\ln Q^2)^2. \quad (28)$$

This equation is nearly coincides with the QCD fit in the kinematics range of these calculations.

The predictions for the small x region measured at HERA shown in Fig.8. It follows from this figure that the initial conditions, based on our knowledge of the Pomeron properties inferred from soft and hard processes, together with conventional QCD evolution, can explain the increase at very small x observed at HERA [3]. Our structure functions compared with the DL [10,20] model, and Multipole Pomeron (MP) [24] with unit intercept. Here Multipole Pomeron means that the Pomeron is a multipole instead of just a simple pole.

The small- x calculated data for the proton structure function $F_2(x, Q^2)$ show that a hard pomeron, with intercept close to 1.3, must be added to the familiar soft pomeron. So the simplest fit to the small- x data corresponds to

$$F_2(x, Q^2) = \sum_{i=0,1} f_i(Q^2) x^{-\epsilon_i}, \quad (29)$$

where the $i = 0$ term is hard pomeron exchange and $i = 1$ is soft pomeron exchange. These parameters (i.e. $f_i(Q^2)$ and ϵ_i) obtained from the best fit to all the small- x data for $F_2(x, Q^2)$ together with the data for $\sigma^{\gamma p}$ [20]. Having concluded that the data for F_2 require a hard pomeron component, it is necessary to test this with our results. We compared our results with the two pomeron fit as is seen in Fig.8. The agreement between our calculated structure function, and its extraction of the hard pomeron fit, is somewhat a striking success both of the hard pomeron concept and of perturbative QCD.

To conclude, in this paper we have obtained a solution of the DGLAP equation for the exponent $\lambda_S(x, Q^2)$ and $\lambda_g(x, Q^2)$ in the next- to- leading order (NLO) at low x . Our results show that of the derivatives $\partial \ln F_2(x, Q^2) / \partial \ln 1/x \equiv \lambda_S(x, Q^2)$ of the proton structure function $F_2(x, Q^2)$ and $\partial \ln G(x, Q^2) / \partial \ln 1/x \equiv \lambda_g(x, Q^2)$ of the gluon distribution $G(x, Q^2)$ are independent of x for $x \leq 10^{-2}$. We see that $\lambda_g > \lambda_S$, as expected by PQCD. We calculated these quantities as a function of Q^2 at fixed x and as a function of x at fixed Q^2 consistent with the $H1$ data [3]. Thus the behavior of F_2 at low x is consistent with a dependence $F_2(x, Q^2) = A_S x^{-\lambda_S}$ throughout that region. At low x , the exponent λ_S is observed to rise linearly with $\ln Q^2$ and the coefficient A_S is independent of Q^2 within the experimental accuracy. This behavior of the structure function $F_2(x, Q^2)$ at low x is consistent with a power- law behavior. Since at low x , $F_2(x, Q^2)$ is primarily driven by the gluon we also expect similar behavior for the gluon. The calculated slopes are consistent with experimental observations. But in the calculations we observed there is a mild x dependency, consistent with the two pomeron model. Our results are compared with the DL and MP modes.

Also we calculated the structure function and the gluon distribution function at low x . We have compared our results with the QCD parton distribution functions. Careful investigation of these results show an agreement with the QCD gluon distributions. The gluon distribution will increase as usual when x decreases. Our results suggest that evolutions both in x and Q^2 have solutions which have strong resemblances to BFKL- like behavior.

References

1. Yu.L.Dokshitzer, Sov.Phys.JETP **46**, 641(1977); G.Altarelli and G.Parisi, Nucl.Phys.B **126**, 298(1977); V.N.Gribov and L.N.Lipatov, Sov.J.Nucl.Phys. **15**, 438(1972).
2. A.De Rujula *et al.*, phys.Rev.D **10**, 1649(1974); R.D.Ball and S.Forte, Phys.Lett.B **335**, 77(1994).
3. H1 Collab., C.Adloff *et al.*, phys.Lett.B **520**, 183(2001).
4. A.V.Kotikov and G.Parente, Phys.Lett.B **379**, 195(1996).
5. J.K.Sarma and G.K.Medhi, Eur.Phys.J.C **16**, 481(2000).
6. P.D.Collins, *An introduction to Regge theory an high-energy physics*(Cambridge University Press, Cambridge 1997)Cambridge.
7. M.Bertini *et al.*, Rivista del Nuovo Cimento **19**, 1(1996).
8. A.V.Kotikov and G.Parente, Phys.Lett.B **379**, 195(1996).
9. E.A.Kuraev, L.N.Lipatov and V.S.Fadin, Phys.Lett.B **60**, 50(1975); Sov.Phys.JETP **44**, 433(1976); *ibid.* **45**, 199(1977); Ya.Ya.Balitsky and L.N.Lipatov, Sov.J.Nucl.Phys. **28**, 822(1978).
10. A.Donnachie and P.V.Landshoff, Z.Phys.C **61**, 139(1994); Phys.Lett.B **518**, 63(2001).
11. A.M.Cooper- Sarkar and R.C.E.D Evenish, Acta.Phys.Polon.B **34**, 2911(2003).
12. W.Furmanski and R.Petronzio, Phys.Lett.B **97**, 437(1980); Z.Phys.C **11**, 293 (1982).
13. R.K.Ellis, Z.Kunszt and E.M.Levin, Nucl.Phys.B **420**, 517(1994).
14. R.K.Ellis , W.J.Stirling and B.R.Webber, *QCD and Collider Physics*(Cambridge University Press)1996.
15. M.Gluk, E.Reya and A.Vogt,Z.Phys.C **67**, 433(1995); Eur.Phys.J.C **5**, 461(1998).
16. H1 Collab., C.Adloff *et al.*, Eur.Phys.J.C **21**, 33(2001).
17. A.D.Martin, R.G.Roberts, W.J.Stirling and R.S.Thorne, Phys.Lett.B **531**, 216(2002).
18. A.Donnachie and P.V.Landshoff, Phys.Lett.B **550**, 160(2002); R.D.Ball and P.V.Landshoff, arXiv:hep-ph/9912445.
19. P.Desgrolard, A.Lengyel and E.Martynov, J.High Energy Phys. **0202**, 029(2002).
20. P.V.Landshoff, hep-ph/0203084.
21. A.V.Kotikov and G.Parente, Nucl.Phys.B **549**, 242(1999); hep-ph/0207276.
22. P.Desgrolard, A.Lengyel and E.Martynov, Eur.Phys.J.C **7**, 655(1999); P.Desgrolard and E.Martynov, Eur.Phys.J.C **22**, 479(2001); J.R.Cudell and G.Soyez, Phys.Lett.B **516**, 77(2001).
23. A.Capella *et al.*, Phys.Lett.B **337**,358(1994); Phys.Rev.D **63**, 054010(2001).
24. L.Csernai *et al.*, hep-ph/0112265.

Figure Captions

Fig.1. Exponents λ_g plotted against x at four fixed Q^2 values and compared with $\lambda_g = \partial \ln G(x, Q^2) / \partial \ln(1/x)$ of MRST2001[17] fit.

Fig.2. Calculation of the exponent λ_g from fits of the form $G(x, Q^2) = A_g x^{-\lambda_g}$ to the our gluon distribution data for $x \leq 0.01$.

Fig.3. The gluon distribution given by Eq.(17) against x at four fixed Q^2 values and compared with NLO-GRV[15](Solid line) , DL fit[18](Dash line) and MRST fit[17](Dot line).

Fig.4. Exponents λ_S plotted against x at four fixed Q^2 values and compared with data from $H1$ [3]. The error bars represent the statistical and systematic uncertainties added in quadrature.

Fig.5. Exponents λ_S plotted against Q^2 at different fixed x values and compared with data from $H1$ [3]. The error bars represent the statistical and systematic uncertainties added in quadrature.

Fig.6. Calculation of the exponent λ_S from fits of the form $F_2(x, Q^2) = A_S x^{-\lambda_S}$ to the our structure function data for $x \leq 0.01$ and compared with data from $H1$ [3]. The error bars represent the statistical and systematic uncertainties added in quadrature . Solid line is the Capella [23] fit with the "bare" Pomeron intercept.

Fig.7. Calculation of the coefficient $A_S(Q^2)$ from fits of the form $F_2(x, Q^2) = A_S x^{-\lambda_S}$ to the our structure function data for $x \leq 0.01$ and compared with data from $H1$ [3]. The error bars represent the statistical and systematic uncertainties added in quadrature.

Fig.8. The calculated values of the structure function $F_2(x, Q^2)$ plotted as functions of x in our method, compared with NLO QCD fit to the $H1$ data [16](solid line), two- pomeron fit [20](dash line), and Multipole Pomeron exchange fit (MP model)[24].

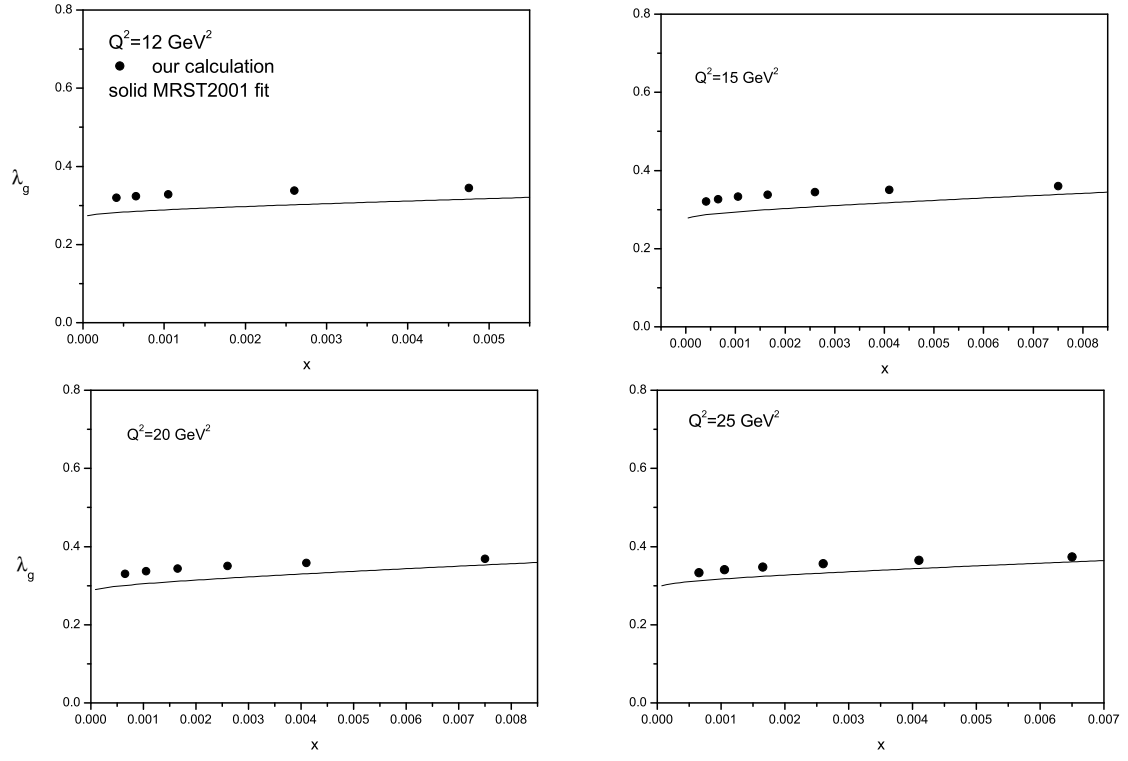


Fig.1

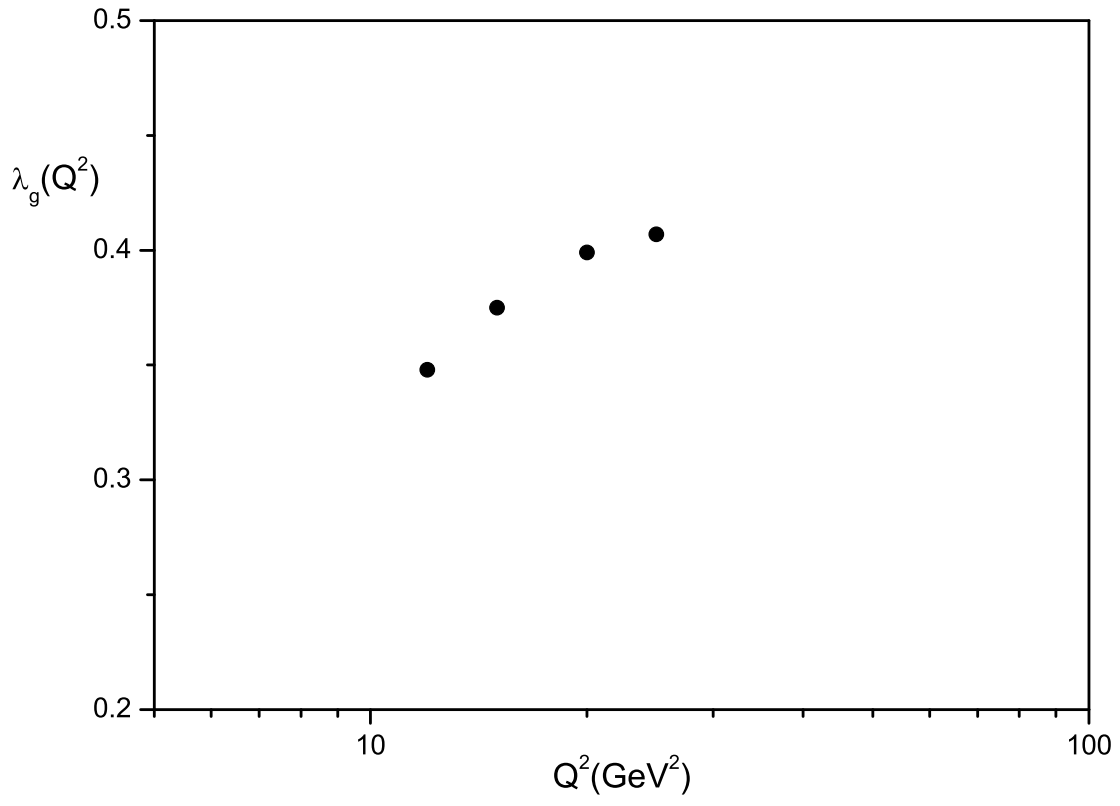


Fig.2

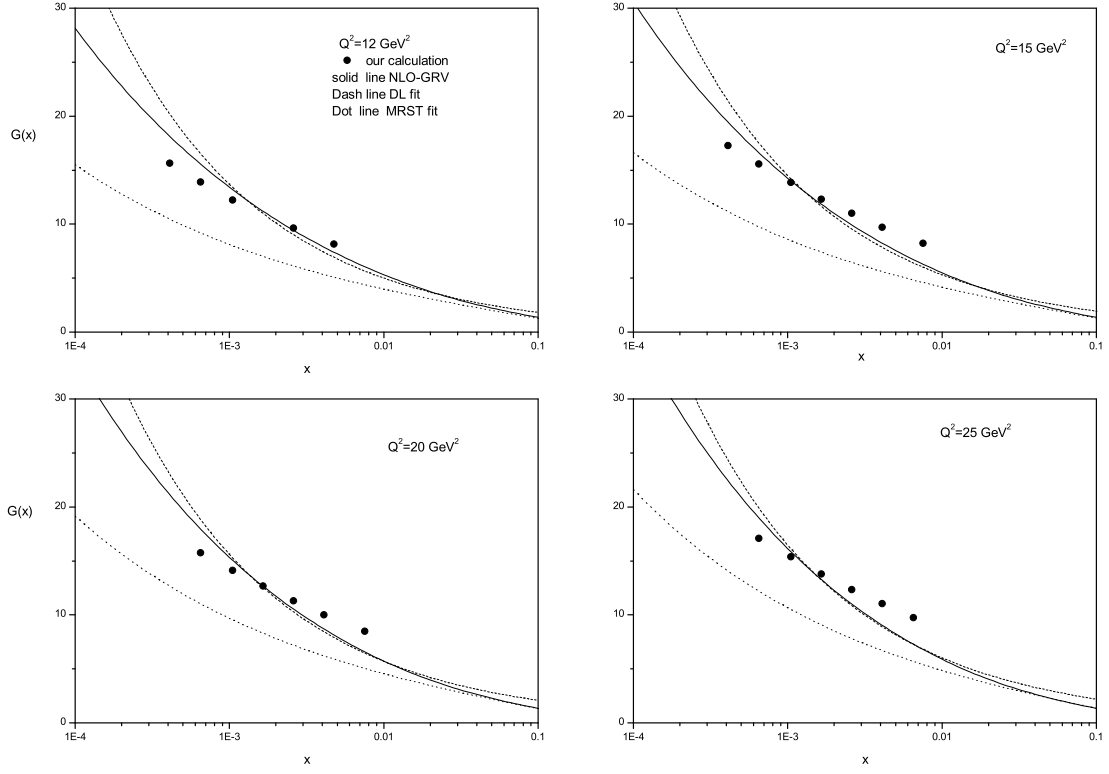


Fig.3

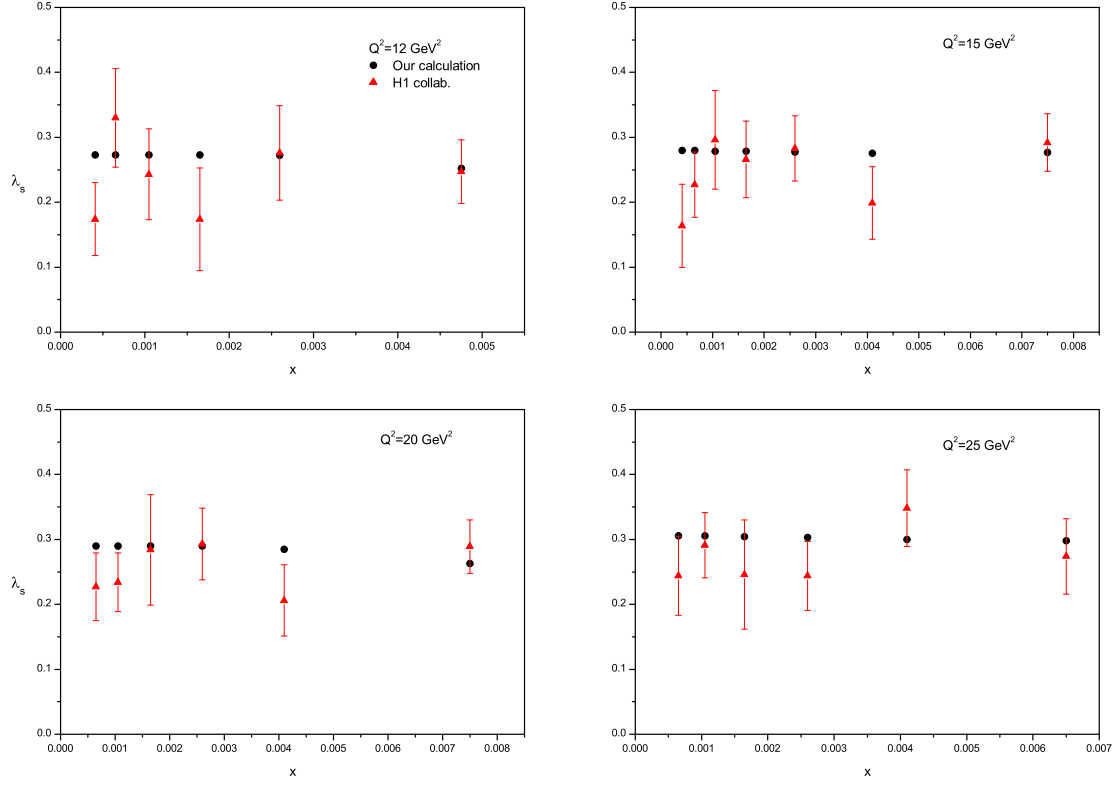


Fig.4

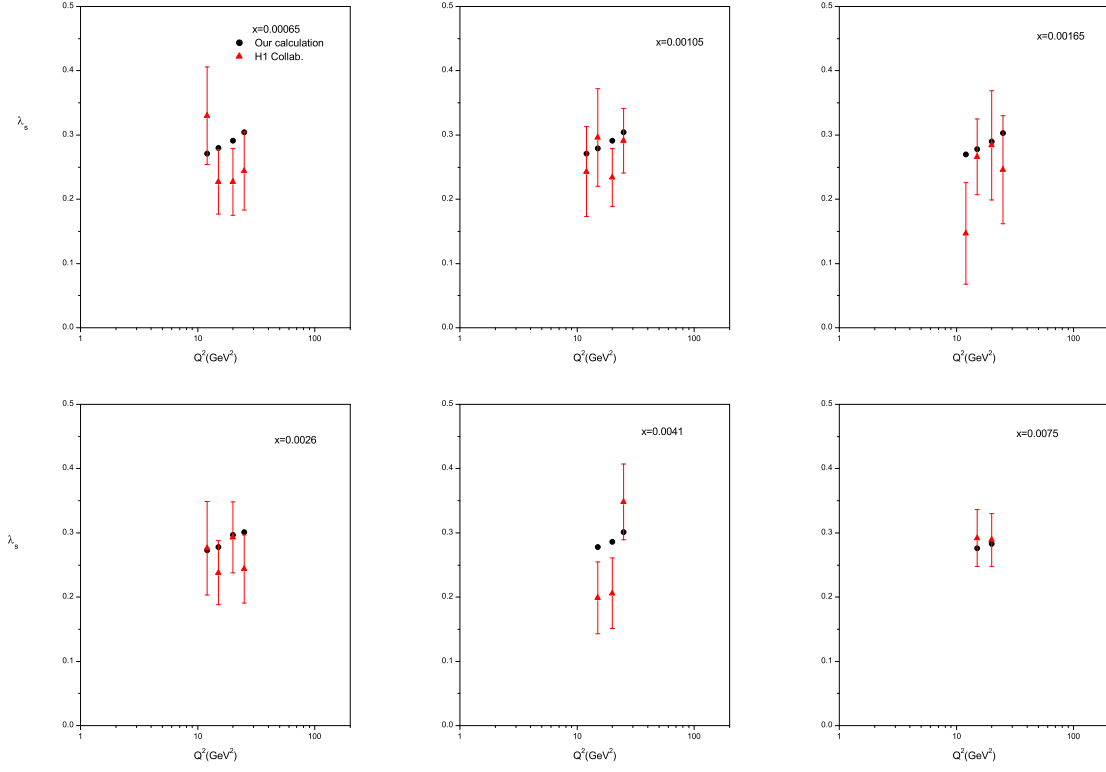


Fig.5

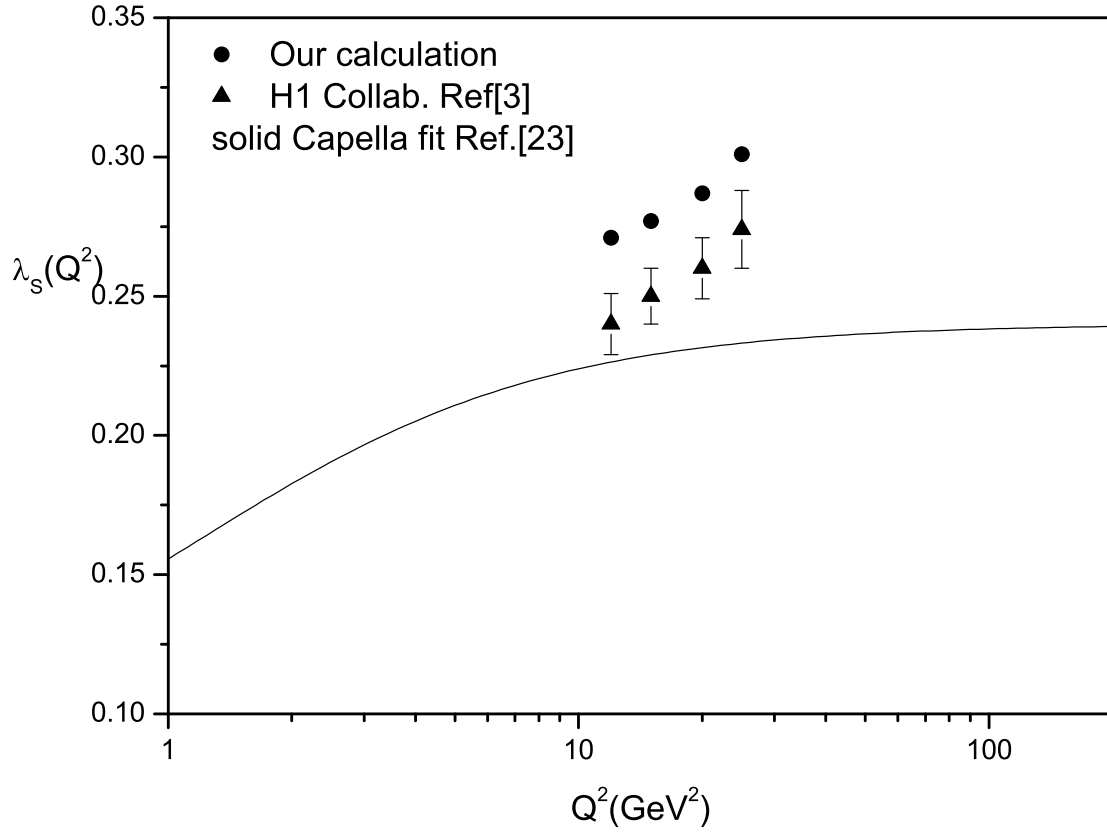


Fig.6

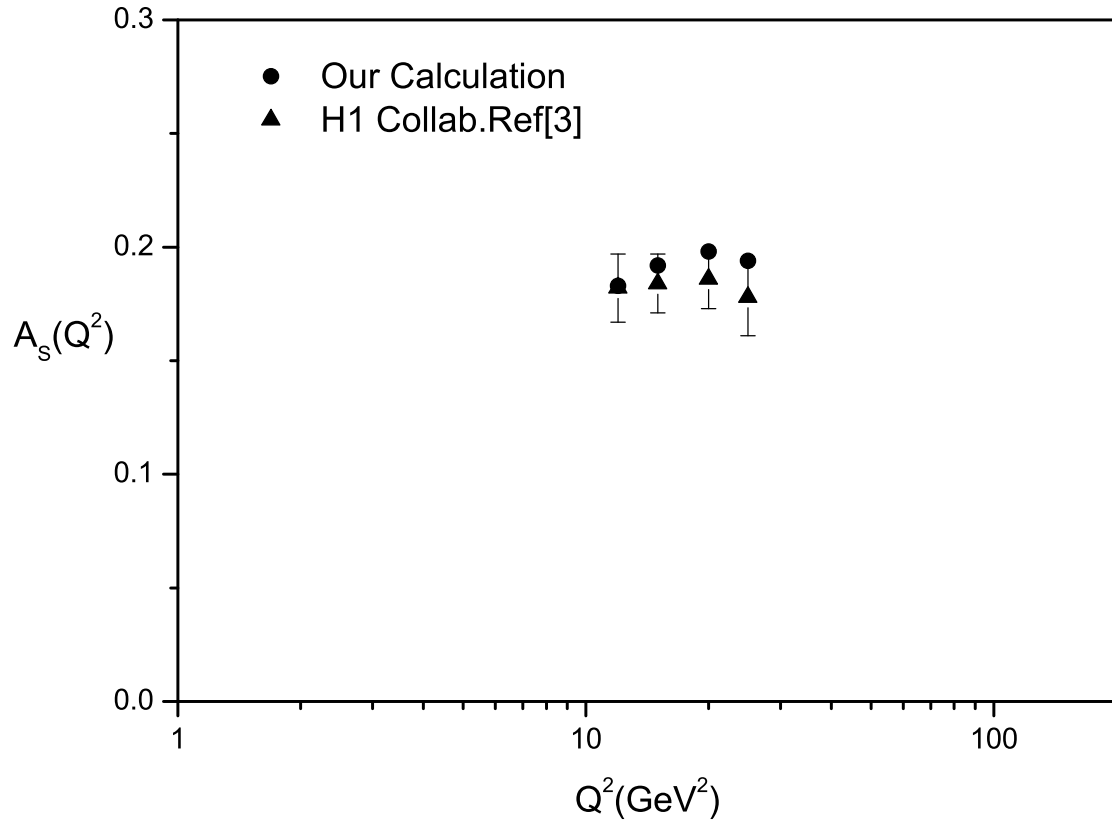


Fig.7

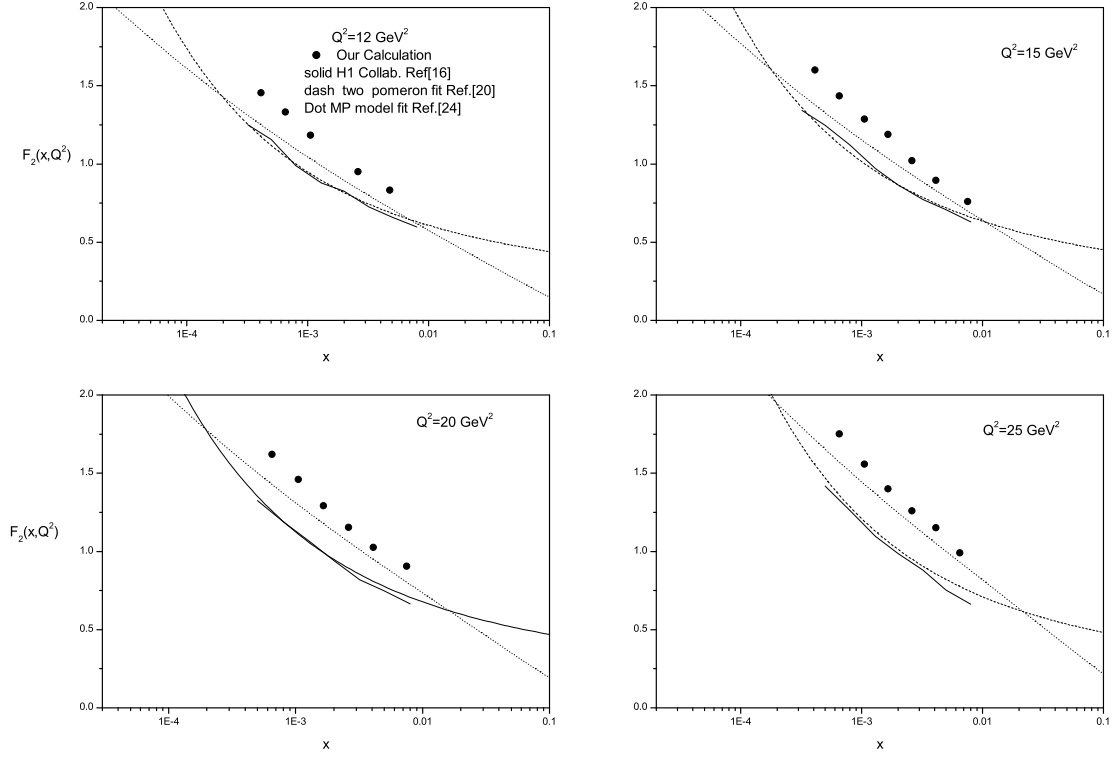


Fig.8